Author's preprint version of the article:

Source apportionment of PM2.5 chemically speciated mass and particle number concentrations in New York City

Masiol, M., Hopke, P.K., Felton, H.D., Frank, B.P., Rattigan, O.V., Wurth, M.J., LaDuke, G.H.

Published in Atmospheric Environment 148 (2017) 215-229

DOI: http://dx.doi.org/10.1016/j.atmosenv.2016.10.044

The original paper is available at:

https://www.sciencedirect.com/science/article/pii/S1352231016308512?via%3Dihub

Source Apportionment of $PM_{2.5}$ Chemically Speciated Mass and Particle Number Concentrations in New York City

M. Masiol,[1] P. K. Hopke,[1] H.D. Felton,[2] B.P. Frank,[2] O.V. Rattigan[2], M.J. Wurth[2], and G.H. LaDuke[2]

[1] Center for Air Resources Engineering and Science, Clarkson University, Potsdam, NY 13699
[2] NYS Department of Environmental Conservation, Division of Air Resources, Albany NY 12233-3256

ABSTRACT

The major sources of fine particulate matter ($PM_{2.5}$) in New York City (NYC) were apportioned by applying positive matrix factorization (PMF) to two different sets of particle characteristics: mass concentrations using chemical speciation data and particle number concentrations (PNC) using number size distribution, continuously monitored gases, and $PM_{2.5}$ data. Post-processing was applied to the PMF results to: (i) match with meteorological data, (ii) use wind data to detect the likely locations of the local sources, and (iii) use concentration weighted trajectory models to assess the strength of potential regional/transboundary sources. Nine sources of $PM_{2.5}$ mass were apportioned and identified as: secondary ammonium sulfate, secondary ammonium nitrate, road traffic exhaust, road dust/resuspension, fresh sea-salt, aged sea-salt, biomass burning and zinc. The sources of PNC were investigated using hourly average number concentrations in six size bins, gaseous air pollutants, mass concentrations of $PM_{2.5}$, and particulate sulfate, OC, and EC. These data were divided into 3 periods indicative of different seasonal conditions. Five sources were resolved for each period: secondary particles, road traffic, NYC background pollution (traffic and oil heating largely in Manhattan), nucleation, and O_3-rich aerosol. Although traffic does not account for large amounts of $PM_{2.5}$ mass, it was the main source of particles advected from heavily trafficked zones. The use of residual oil had limited impacts on $PM_{2.5}$ mass but dominates PNC in cold periods. These findings are useful for planning air quality mitigation strategies for NYC.

Keywords: Source apportionment; Positive matrix factorization; $PM_{2.5}$ mass concentration; particle number concentration; New York City; Residual oil

1. INTRODUCTION

Epidemiological studies have identified that exposure to increased mass concentrations of airborne particulate matter (PM) leads to multiple adverse health effects (e.g., Turner et al., 2011; Anderson et al., 2012; Loomis et al., 2013; Raaschou-Nielsen et al., 2013). Mass concentration is the standard current metric for measuring and controlling PM exposure. Based on the epidemiology and resulting guidance of international organizations (e.g., WHO, 2000; IARC, 2013), national legislation in many developed countries has fixed thresholds, limits, and/or target values for PM mass concentrations. In the U.S., air quality is regulated using National Ambient Air Quality Standards (NAAQS) that set limit values to be attained across the U.S. for PM with aerodynamic diameters less than 10 and 2.5 μm (PM_{10} and $PM_{2.5}$, respectively).

Although the NAAQS are designed to reduce the adverse effects of PM on health, recent population-based studies have reported that even the exposure to low mass concentrations may increase acute and chronic effects and mortality (Shi et al., 2015). Since smaller particles may be more effectively deposited in the lung (Salma et al., 2015), mass concentrations could be an inefficient metric for the potential excess mortality and morbidity associated with PM. However, currently there is limited knowledge of the specific components of PM (size, number, source, composition) that drive the health outcomes (Atkinson et al., 2010).

The present study investigated the major sources of $PM_{2.5}$ in the NYC area through the application of receptor models to two particulate metrics: mass concentration and particle number concentration (PNC). The most probable sources of $PM_{2.5}$ mass were identified and apportioned using positive matrix factorization (PMF) with 24-hour chemically speciated sample data. The sources of PNC were also investigated by applying PMF to hourly average particle number concentrations resolved into six size bins (20-30 nm, 30-50 nm, 50-70 nm, 70-100 nm, 100-200 nm, 200 nm to 2.5 μm), gaseous air pollutants and $PM_{2.5}$ mass concentrations, and particulate sulfate, OC, and EC. Subsequent analyses included: (i) the comparison of sources identified over mass and particle number concentrations through correlation analyses; (ii) the use of wind data through polar analysis to detect the directions of the probable local sources; and (iii) the use of an air parcel back trajectory method to estimate the strengths of potential distant sources.

2. MATERIALS AND METHODS

2.1 Study area

New York City (NYC) is the most populous city in the U.S. with approximately 8.5 million inhabitants within its five boroughs and almost 20 million inhabitants in the New York metropolitan area. Despite attaining the NAAQS for ambient PM, it was estimated that ambient $PM_{2.5}$ still contributes to >3000 annual deaths, 2000 hospital admissions for lung and heart conditions, and approximately 6000 emergency department visits for asthma (NYC Department of Health and Mental Hygiene, 2013a,b).

2.2 Experimental

Measurements were made within the NYC metropolitan area at the NYS Department of Environmental Conservation air quality monitoring site at Queens College (QC: 40° 44.225'N; 73° 49.295'W; 24 m a.s.l.). This site is located in a high population density section of Queens County (Figure 1). Nitrogen oxides ($NO+NO_2 \equiv NO_x$), sulfur dioxide (SO_2), ozone (O_3), and carbon monoxide (CO) using EPA equivalent or reference methods. Details are provided in supplementary information section S1. $PM_{2.5}$ mass concentrations were measured with a tapered element oscillating microbalance/filter dynamics measurement system (TEOM/FDMS) that provides both semivolatile and nonvolatile PM concentrations.

In addition, $PM_{2.5}$-speciated data measured at QC were obtained from the EPA Chemical Speciation Network (CSN) (AQS, www.epa.gov/aqs). Samples were collected every third day and analyzed for major inorganic ions (Na^+, K^+, ammonium, nitrate, sulfate) by ion chromatography, elemental carbon (EC) and organic carbon (OC) by thermo-optical analysis, and elements with atomic number ≥11 by energy-dispersive x-ray fluorescence (EDXRF). Details of the CSN network sampling, analyses and quality assurance are described by Solomon et al. (2014). Data at QC are available from 2001 to the present.

Hourly concentrations of additional air pollutants were recorded at QC between June 2009 and July 2010. PNC were measured in six size bins (20-30 nm, 30-50 nm, 50-70 nm, 70-100 nm, 100-200 nm, 200 nm to 2.5 μm) with a TSI model 3031 particle monitor. Methane (CH4) and non-methane hydrocarbon (NMHC) were analyzed using a flame ionization detector (Horiba model APHA-360). Particulate sulfate was measured with a Thermo Scientific model 5020i. Particulate OC and EC was determined with a semi-continuous carbon aerosol analyzer (Sunset Lab., Tigard, OR, USA) operating a modified NIOSH 5040 protocol (Bauer et al., 2009).

QC is affected by typical anthropogenic sources of densely inhabited urban environments. Road traffic is ubiquitous in this area and frequently congested major roads such as the Long Island Expressway are adjacent to the site. Natural gas and number 2 oil are the primary fuels for domestic and small building heating in NYC. Many large buildings used residual oil in their central heating systems particularly in Manhattan (Peltier et al., 2009). There are ship emissions from passenger ferries in the New York–New Jersey harbor and from the large container terminal at the Port of Elizabeth, Newark NJ. Finally, there are aircraft emissions released at the two major airports in NYC: JFK (~8.5 km SSE) and LaGuardia (~4.8 km NW).

2.3 PMF Analyses

PMF is described elsewhere (Paatero and Tapper, 1994; Paatero, 1997; Hopke, 2015; 2016) and in supplementary material section S2. US EPA PMF version 5 was used because it has two new features: (i) displacement (DISP) analysis, which is designed to explore the realistic bounds on the optimal (base run) solution that do not result in appreciable increases in the Q values and (ii) constraints that can be applied to the solutions to utilize a priori information about the nature of the profiles or contribution values and reduce rotational ambiguity (Brown et al., 2015).

Since PMF requires concentrations and their associated uncertainties, several strategies were used to estimate the uncertainty for each variable. Details are provided in supplementary material section S3. The total variable (total PNC) was calculated by summing the number concentrations over the six channels. Total PNC was assigned an uncertainty of 300% and also marked as "weak" to avoid it driving the model (Kim et al., 2003).

The best solutions were identified based on (Reff et al., 2007; Belis et al., 2014; Brown et al., 2015; Hopke, 2016): (i) knowledge of sources impacting the study area, (ii) the *Q-value* with respect to the expected (theoretical) value and its stability over multiple (n=100) runs, (iii) number of absolute scaled residuals over ±3, and (iv) finding profile uncertainties calculated by bootstrap (BS, n=300) and displacement (DISP) methods within an acceptable range (Paatero et al., 2014). In this study, the ranges calculated by DISP for the dQ=4 were used to assess the uncertainty boundaries associated to the final PMF profiles.

126 ## 2.4 Meteorology and related models

127 Ambient air temperature, wind speed and direction, relative humidity and atmospheric
128 pressure were recorded hourly at LaGuardia (LGA) airport (Figure 1 and SI1). Back-trajectories
129 were obtained using the NOAA/ARL hybrid single particle Lagrangian integrated trajectory
130 (HYSPLIT4) model (Stein et al., 2015; Rolph, 2016). Back trajectories were calculated for 96 h
131 with a starting height of 500 m a.g.l. and the NCEP/NCAR Reanalysis database.

132 The potential local source locations were assessed using bivariate polar plots: these polar
133 plots show the average pollutant concentrations by mapping wind speed and direction as a
134 continuous surface and surfaces calculated using smoothing techniques. Details are provided by
135 Carslaw et al. (2006) and Carslaw and Ropkins (2012). Polar plots were applied to the PMF
136 contributions for both the daily $PM_{2.5}$ mass and hourly PNC concentrations. Hourly PNC data
137 were analyzed using the concurrent hourly wind data. For the 24-h $PM_{2.5}$, the same mass
138 concentration was assigned to each of the 24 hourly wind direction values (Kim and Hopke,
139 2004).

140 The potential locations of distant sources were assessed using concentration weighted
141 trajectory (CWT) analysis (Stohl, 1998). CWT weights trajectories with their associated
142 concentrations (Stohl, 1996; Lupu and Maenhaut, 2002; Hsu et al., 2003: Squizzato and Masiol,
143 2015). The details are summarized in supplementary material section S4.
144
145 # 3 RESULTS
146 ## 3.1 Source apportionment using chemically speciated $PM_{2.5}$

147 Because of the limited number of samples (1 sample collected every 3 days), 2 years
148 (April 2009-March 2011) of data were analyzed. The selected period includes the PNC campaign
149 (June 2009- June 2010), but the additional time provided more stable results. Days with
150 anomalously high concentrations due to known events (e.g., New Year's and Independence Day)
151 were excluded. Based on the S/N ratios, 14 species were categorized as "strong" (nitrate, sulfate,
152 ammonium, EC, OC, Na, Si, Cl, K, Ca, Fe, Ni, Cu, Zn), while 4 were marked as "weak" by
153 tripling their uncertainties (Al, V, Mn, Br). Total K was preferred to its ionic species (K^+); total
154 sulfur was excluded because of its high correlation with sulfate (r=0.97). $PM_{2.5}$ was included as
155 total variable and marked as "weak." An addition of 5% uncertainty was included to encompass
156 errors not considered in the uncertainty assessment.

The seasonal distributions of the variables are shown in supplementary material Figure SI2. Nitrate, Na, Cl, K, Ca, Mn, Ni, Cu and Zn show highest median values in winter, while sulfate and OC are highest in summer. $PM_{2.5}$ was high in both summer and winter. Al, Si are highest in spring while V and Fe are constant over the year.

Solutions were explored from 3 to 12 factors. The most physically plausible results were obtained with a 9-factor solution that also had a Q closest to the theoretical (Q_{exp}) value (Q_{true}/Q_{exp}=0.94). Good PMF diagnostics were found, i.e.: (i) all runs converged; (ii) all species had stable Q values over 100 repeated base runs; (iii) low values for the sum of the squares of the differences in scaled residuals for each base run pair by species were obtained; (iv) all scaled residuals were symmetrically distributed; and (v) modeled total variable ($PM_{2.5}$) was successfully predicted ($R^2 > 0.9$). No edges were found in the G-space plots (Paatero et al., 2005), and therefore, FPEAK solutions were not investigated. However, constraints were applied to V (maximally pulled up in factor 8 and pulled down in factor 4). A series of different constraints were investigated involving various elements and factors. The constraint allowed: (i) better resolution of the factors sharing V; (ii) fewer swaps in BS; and (iii) higher explained variation of V into its main factor, resulting in an easier interpretation. Despite these advantages, the constrained solution had minor changes in the final solution: $dQ \leq 1\%$ with respect to the base run and negligible changes in the profiles for remaining species. BS and DISP were thus applied to the constrained solution: no factor swaps occurred for DISP analysis indicating that there are no significant rotational ambiguities and the solutions are sufficiently robust; (vi) no unmapped factors and no swaps occurred on constrained solution over a total of 100 BS runs.

The resulting profiles are presented in Figure 2 and the time series of contributions is shown in Figure SI3. The contributions were also aggregated to show monthly and weekly averages (Figure 3). The polar plot and CWT analyses are shown in Figures 4 and 5, respectively.

3.1.1 Secondary ammonium sulfate

The first factor accounts for 34% of total annual $PM_{2.5}$ mass concentration (DISP range 28-48%) and shows very high explained variation for sulfate (77%) and ammonium (62%), but also significant fractions of bromine (21%), OC (16%) and V (10%). Sulfate in NYC is typically due to emissions of SO_2 by coal-fired power plants in the upper Ohio River Valley (Dutkiewicz

et al., 2003; Hopke et al., 2005). Another source of sulfate in coastal environments is biogenic and sea salt sulfate (Barnes et al., 2006). Factor 1 represents secondary ammonium sulfate. Hand et al. (2012a, b) estimated that sulfate PM accounts for 30–60% of monthly average $PM_{2.5}$ mass in the Eastern U.S. The factor had its highest concentrations in the warmest season (June-August). Despite the weekly pattern that shows a minimum on Saturdays, the nonparametric Kruskal-Wallis analysis of variance indicates no statistically significant (p<0.05) variations through the week. The polar plot analysis exhibits increased values when moderate winds (speed 3-9 m s^{-1}) blow from the SW. This pattern is compatible with the CWT results, showing higher average levels related to probable transport from the Ohio River Valley such as has been seen in many prior studies (e.g., Dutkiewicz et al., 2003; Li et al., 2004).

3.1.2 Secondary ammonium nitrate

Factor 2 is mainly composed of nitrate (74%) and ammonium (24%), but also bromine (17%). It is strongly correlated with NO_2 (r=0.65) and weakly (0.5<r<0.6) with particles in the 30-200 nm range. It represents secondary ammonium nitrate (NH_4NO_3) (Seinfeld and Pandis, 2006). Annually, it accounts for 12% (10-24%) of total $PM_{2.5}$ mass, but shows significant higher concentrations during winter and no statistically significant weekly patterns. The seasonal pattern is linked by the kinetics of formation of ammonium nitrate: (i) the chemistry of NH_4NO_3 competes with ammonium sulfate, which is generally more thermodynamically stable (Pinder et al., 2008), but is favored by cold temperatures and high relative humidity (Stelson and Seinfeld, 1982); and (ii) nitrate partitioning leans toward the gaseous phase at temperatures above 20°C (Schaap et al., 2004). The polar plot shows higher average concentrations when slow and moderate winds blow from W-S sectors; CWT reveals a probable source area over the Ohio River Valley.

3.1.3 Fresh sea-salt

Factor 3 is assigned as fresh sea-salt. It accounts for 1% of $PM_{2.5}$ mass (1-2%), but with high explained variations for chlorine (82%) and sodium (19%). It also includes nitrate, sulfate, ammonium, EC, OC and Fe accounting for <4% of percent of species sum. The DISP bounds show that their values include zero, supporting the assignment of sea-salt. The Na/Cl ratio in the profile (0.61) is close to that of seawater (0.56), confirming a limited chlorine depletion. The

time series of Factor 3 contributions does not show clear seasonal and weekly patterns. Slightly higher concentrations are recorded in winter probably due to East Coast winter cyclones (northeasters) and their consequent storm surges affecting the coastline (e.g., Colle et al., 2008). The presence of moderate amounts of Al and the wide DISP range for Si could be linked to the presence of crustal particles dispersed in seawater, but could be also linked to the use of road salt in winter (Al and Si are also tracers of road dust resuspension). However, the analysis of the time-series (Figure SI3) shows that this factor presents some one-day high peaks likely due to sea storm events instead of road salt resuspension. Polar plot analysis further supports this interpretation by showing increased concentrations for very strong winds from Long Island Sound and the Atlantic Ocean compatible with the local production of marine aerosol from wind-induced bubble bursting at the sea surface (Lewis and Schwartz, 2004). The CWT clearly indicates its main origin from coastal areas in the northeastern U.S.

3.1.4 Aged sea-salt

Factor 4 accounts for 9% (3-14%) of $PM_{2.5}$ mass concentration and has high shares of sodium (81%), but also significant shares of bromine (21%), OC (10%), sulfate (13%), and nitrate (9%). As for factor 3, sodium is a typical tracer for sea-salt, but in this case chlorine is missing, while sulfate and nitrate are overabundant. It has been largely demonstrated that sea-salt aerosol may show strong chloride deficiencies compared to the original seawater composition (Keene et al., 1999; Rossi, 2003) after ageing in the atmosphere. The chloride depletion is attributed to reaction of alkali halides with HNO_3 and H_2SO_4 in the gaseous or aqueous phases (ten Brink, 1998; Song and Carmichael, 1999). The CWT indicates a probable origin from coastal areas in the southeastern U.S.

3.1.5 Road traffic emissions

Factor 5 depicts road traffic emissions. It accounts for 16% of $PM_{2.5}$ mass (10-25%) and high percentages of EC (52%) and OC (34%) that represent primary engine exhaust. The factor also includes V (30%), Mn (27%), Fe (56%), Cu (66%). The latter three metals are strongly related to road traffic emissions (e.g., Adachi and Tainosho, 2004; Harrison et al., 2012; Pant and Harrison, 2013), while V is found in residual oil (Osan et al., 2000) and related fuels. Significant positive correlations with $r > 0.5$ are found with NO_x (particularly NO), CO, methane, and EC

(particularly opt.EC). Correlations >0.6 are also found with PNC from 70 to 200 nm in size. Road traffic contributes to a large range (30-200 nm) of particle number size distributions in urban atmosphere (e.g., Constabile et al., 2009). Weekly patterns are also typical of road traffic showing slight decreases during weekends (when less truck traffic is expected in NYC). Polar plot analysis shows increased values during wind calm periods, compatible with a local source, and low wind speeds from SSE, i.e. toward central Brooklyn.

3.1.6 Crustal material

Factor 6 accounts for high percentages of Al (80%), Si (80%) and moderate (14-23%) of K, Ca, Mn and Fe, markers of crustal origin although in urban areas, such particle arise largely from suspension from roads by traffic and construction activities. It accounts for 3% (3-15%) of $PM_{2.5}$ mass. The factor showed no weekly cycles, but had higher concentrations in the spring and summer. Similar to road traffic emissions, the polar plot shows higher values with moderate winds from the south.

3.1.7 Biomass burning

Factor 7 accounts for 16% (11-32%) of $PM_{2.5}$ mass and is made up of K (43%), OC (37%), Br (33%), EC (11%) and Ca (9%). Soluble potassium is a strong marker of biomass combustion. Biomass burning aerosol consists of a non-uniform mixing of high molecular weight organics, soot and potassium (e.g., Lee et al., 2015). In U.S., biomass burning is relevant in summer due to wildfires (Wang et al., 2010) and in winter from domestic wood burning (e.g., Wiedinmyer et al., 2006; Wang et al., 2012a,b; Zhang et al., 2014). This factor exhibits a weak seasonality with increased winter concentrations, which is compatible with recreational wood combustion. The weekly cycles show weak peaks on Sundays (but not statistically significant), compatible with increased residential wood combustion in winter and barbeques in summer. The factor shows weak correlations ($0.5<r<0.6$) with 70 to 200 nm PNC, that are common for wood smoke (Chandrasekaran et al., 2013). The polar plot does not indicate a prevailing direction, but higher concentrations are observed during high wind speeds. The CWT shows increasing concentrations when air masses pass over the Ohio River Valley and the boreal forests of eastern Canada.

3.1.8 Residual oils/domestic heating

Factor 8 has high explained variations of vanadium (48%), nickel (70%) and also moderate values for Ca (40%), Mn (32%), EC (23%) and Fe (21%). Its annual contribution to the $PM_{2.5}$ mass is 3% (1-15%), but strongly increases during winter (December-February) with no evident weekly patterns. Nickel and vanadium are key tracers for residual oil combustion (Moreno et al., 2010) including heavy fuel oil boilers (Sippula et al., 2009), petrochemical refineries (Bosco et al., 2005; Sanchez de la Campa et al., 2011), coke production (Moreno et al., 2007) and shipping emissions (Moldanova et al., 2009; Becagli et al., 2012). Sources present in the NY-NJ area include:

- Residual oil combustion is a known source of particulate nickel in NYC (Peltier et al., 2009). No. 4 and No. 6 oils were used in large building heating systems: No.6 oil has high sulfur concentrations (3000 ppm), Ni (~17 ppm), V (3 ppm), Mn (2.9 ppm) and Zn (1.9 ppm) (NYSERDA, 2010).
- No.4 and 6 oils were regulated in 2011 to transition to No.2 oil. Earlier studies (e.g., Huffman et al., 2000) have shown that $PM_{2.5}$-bound Ni and V emissions from residual fuel oils boilers are predominantly present as sulfates ($NiSO_4$ and vanadyl sulfate, respectively);
- There is a large oil refinery just south of Elizabeth, NJ (~35 km WSW of QC);
- Ship emissions are present in the area from the NY-NJ harbor with the container port at the Port of Elizabeth, NJ. Vanadium was also strongly associated with ship emissions in NYC (NYCCAS, 2016a);

Strong correlations with NO_x (r=0.75), SO_2 (r=0.84), NMHCs (r=0.64), and particles in the nucleation and Aitken size ranges (<100 nm) support factor 8 being local combustion sources. Polar plot analysis shows increasing concentrations when moderate to high (5-10 m s^{-1}) winds blow from the N-W, i.e. Manhattan. This results correlated with the map of Ni concentrations developed for NYC (NYCCAS, 2016b) showing that the higher levels of Ni were found in locations near to units burning No.4 or No.6 oil and in areas with high residential population density. This way, the most probable source is residual oil combustion in Manhattan. However, the polar plot also shows increasing levels with high (10 m s^{-1}) ESE winds.

311 *3.1.9 Zinc*

312 Factor 9 contributes to 4% (2-12%) of $PM_{2.5}$ mass with highest contributions in winter. It
313 is dominated by the explained variation of Zn (79%) with moderate values for Ni (27%), Ca
314 (20%), Cu (14%), Mn (13%) and K (11%). However, only Zn, Cu and Mn show DISP ranges
315 that never reach zero. Zinc is a known tracer for lubricating oil combustion (Kleeman et al.,
316 2008) as well as brake and tire wear along with Mn, Fe and Cu (Harrison et al., 2012; Pant and
317 Harrison, 2013). Zn accounts for around 1% by weight of tire tread and is a significant source of
318 Zn (Thorpe and Harrison, 2008). However, the relatively high DISP ranges of OC, Si, and Ca
319 could represent pavement wear. The polar plot analysis shows a potential source to the NE with
320 moderate winds (>7 m s^{-1}), i.e. toward two major roads (Horace-Harding and Van Wyck
321 Expressways). Thus, the factor could be road dust.

322 However, the factor also has a strong correlation with SO_2 (r=0.68) and increasing
323 correlations as particle sizes becomes smaller (<50 nm), which poorly match with this latter
324 interpretation and, suggests a combustion source. Mass-relevant contributions from abrasion
325 particles and resuspended road dust mainly peak in the coarser ranges, i.e. 1–10 μm (Bukowiecki
326 et al., 2010). The factor cannot be also associated to on-road diesel trucks since the use of
327 ultralow S fuel in U.S. began in 2006. It has a strong seasonal pattern with high concentrations in
328 the winter so it may space heating. Zn was found as a prevailing metal in No.2 oils, which also
329 contain 15 ppm sulfur and 3.2 ppb Ni (NYSERDA, 2010). Thus, the interpretation of factor 9
330 remains unclear, but may represent a second building heating source.
331

332 **3.2 Source apportionment of particle number concentrations**

333 Descriptive statistics, seasonality, daily cycles and relationships among the measured
334 species are discussed by Masiol et al. (2016 submitted). Since photochemical activity has a key
335 effect on driving particle size and it changes according to the solar irradiation, the best results of
336 source apportionment studies on particle size spectra data can be extracted by splitting the
337 dataset seasonally (Zhou et al., 2004). Thus, PMF was run separately for winter, summer and
338 transitional seasons. Seasons were selected by reviewing the air temperature and solar irradiation
339 variations. Winter was 16th November to 15th March, summer from16th May to 15th September
340 and transitional (remaining periods). Seasonal wind roses are provided in Figure SI1.

Cumulative variables (NO_x, THC, TC) were excluded from the datasets because they were not linearly independent. Methane and NMHCs were excluded from the summer dataset because of a high number of missing values. The final datasets included 18 variables for winter and transitional periods and 16 for summer. An additional 8-10% uncertainty was added to the models to encompass errors not considered in the uncertainty assessment. Based on the S/N criterion, all of the variables were inputted as "strong" for the winter dataset. NMHC was included as "weak" for the transition period. SO_2 and CO were categorized as "weak" in summer. In addition, OC was also inputted as "weak" in summer due the possible artifacts related to the evaporation of the most volatile fractions of the organic matter.

PMF solutions from 3 to 8 sources were examined. The most stable, robust, and interpretable results were found with 5-factor solutions for each period. The solutions yielded stable, reliable diagnostics, i.e.: (i) all runs converged; (ii) species had stable *Q* over 100 repeated base runs and low values for the sum of the squares of the differences in scaled residuals for each base run pair by species; (iii) all scaled residuals were symmetrically distributed indicating good fits to the data; (iv) a few cases showed absolute scaled residuals exceeding ±3, indicating the presence of potential outliers; (v) modeled total variable (total PNC) was successfully predicted for every period ($R^2 > 0.9$ and slopes≈1); (vi) no factor swaps occurred for DISP analysis indicating that there are no significant rotational ambiguities; (vii) all factors had >98% in mapping from the BS run (*n*=300), suggesting that the BS uncertainties can be reasonable and the selected number of factors is appropriate; and (viii) BS-DISP had no swaps at any *dQ* when selecting all strong variables for displacement. The potential for rotational ambiguity was also checked using the G-space plots and by running over multiple FPEAK solutions (range -10 to +10, step 0.1). FPEAK= 0 was selected for all the seasons. Rotational uncertainties were further assessed through the analysis of DISP ranges. A slight constraint was applied to the summer results by pulling up $PM_{2.5}$ in factors 2 and 4. Constraints resulted in a negligible variation in *%dQ* (<1), but provided more interpretable profiles.

Generally, all periods returned similar source profiles. The extracted factor profiles and diurnal patterns are shown in Figures 6, SI4, and SI5. Day of week patterns are provided as Figure SI6. The contributions to total PNC are summarized in Table 2, polar plots are shown in Figure 7 and selected CWT maps in Figure 8. The interpretation of factors was more difficult than in prior size distribution analyses because of the much lower number of size channels (6

372 compared to 52). The relationships of the PMF analysis of the speciated data were assessed with
373 Pearson' correlation analysis using daily averaged factor contributions (Table 3).
374
375 *3.2.1 Winter*
376 The first factor showed limited contributions to the total PNC (DISP range 3-4%).
377 Although the profile shows modes in the nucleation (20-30 nm) and accumulation (100-200 nm)
378 size ranges, the percentage contributions of species increases as particle size increases. Despite
379 the low contribution to the total PNC, factor 1 contributes to the PM mass (this is also confirmed
380 by the high explained variations of $PM_{2.5}$, sulfate, and OC). Its diurnal pattern shows a broad
381 minimum during daytime, which is more likely related to the mixing layer height dynamics than
382 variations in source emissions. Factor 1 is interpreted as secondary inorganic and organic
383 aerosol. It is slightly but statistically lower on Saturdays (Kruskal-Wallis $p<0.05$). The polar plot
384 showed increases from all directions under low winds (<5 m s^{-1}) and from SW at moderate
385 speeds, i.e., directionality similar to secondary sulfate for $PM_{2.5}$ mass (Figure 4). It also has
386 strong positive correlations with secondary aerosol sources extracted by the prior PMF results
387 (Table 2). The CWT map points out the northcentral U.S. in winter shifting toward the Ohio
388 River Valley in summer as strong potential source regions.
389 Factor 2 contributes to 2-4% of total PNC. It includes NO (90%) and has significant
390 variation of EC (28%), $PM_{2.5}$, sulfate, OC, CO and SO_2 (10-20%). However, PNC are low in all
391 sizes with a weak mode at 30-50 nm, compatible with spark ignition particle emissions.
392 Daily/weekly cycles reveal a sharp peak between 7-9 am, i.e. during morning rush hours, and a
393 drop during weekends. This factor is strongly correlated with several $PM_{2.5}$sources: ammonium
394 sulfate and nitrate, road traffic and residual oil. The polar plot indicates increased concentrations
395 during calm winds. This factor represents a local source. Primary road traffic emissions are the
396 most likely interpretation since nearby road traffic is intense at QC and NO, EC, OC, CO are
397 pollutants primarily emitted by motor vehicles.
398 Factor 3 is the major source of PNC (47-54%) and exhibits a clear pattern in particle
399 size, increasing with decreasing particle size. This factor also accounts for high percentages of
400 NO_2 (~50%), SO_2 (~50%) and moderate (>33%) EC and NMHCs. NO_x is emitted by high
401 temperature combustion (mostly as NO) with heavy duty diesel trucks and building heating as
402 important sources. NO_2 is formed by reaction with ozone. EC, HMHCs and SO_2 are also emitted

from combustion sources including vehicle emissions, with EC dominant in diesel exhaust compared to spark-ignition vehicles (Zielinska et al., 2004; Lough et al., 2007; Cheung et al., 2009; 2010). The diurnal pattern shows two maxima (6-8 am and 5-10 pm) characteristic of road traffic (morning and evening rush hours), but the morning peak is about 1 h earlier than the maxima observed for factors 2 and 4. This pattern is also consistent with building heating, which typically starts earlier in the day and produces UFPs. The polar plot indicates increases for moderate wind speeds (<7 m s^{-1}) and for winds blowing from the NW (Manhattan). From its directionality, this factor can be linked to a background of pollution arising from multiple sources in NYC, including: (i) road traffic (two diurnal peaks); (ii) harbor activities (high loading of SO_2); and (iii) domestic heating and residual oil combustion in centralized heating systems (early morning peak; high loading for SO_2 and NO_2; strong significant correlation with the residual oil factor of $PM_{2.5}$ PMF analysis (Table 2).

Factors with similar profiles were found in the other seasons. However, the concentrations in winter were significantly higher than in the other periods. The higher winter concentrations may be caused by: (i) ultrafine particles being more persistent in cold weather with lower evaporation after emission; (ii) additional emissions from heating systems; and (iii) lowered mixing layer heights during colder periods reducing pollutant dispersion.

Factor 4 contributes to 35-42% of total PNC and includes a wide particle size range (20-200 nm). It significant contributes to $PM_{2.5}$ mass (21%) with negligible contributions to the other pollutants. Both the daily pattern and polar plot are similar to primary road traffic emissions (factor 2), i.e. a sharp peak during the morning rush hours and increased concentrations for calm winds and for winds blowing from the SW (Brooklyn). Only weak correlations were found with any of the $PM_{2.5}$ factors. Factors 2 and 4 seem to represent sources linked to vehicular traffic. Although this result appears to be factor splitting from too many factors, the split remains for solutions with lower numbers of factors, demonstrating that they represent two distinct sources. Some studies have reported that wintertime nucleation in Northeastern U.S. occurs principally in the morning (e.g., Jeong et al., 2004; Kasumba et al., 2009; Wang et al., 2011) resulting from motor vehicle emissions during morning rush hours. Therefore, this factor is assigned as nucleation and the subsequent particle growth is the result of condensation of semi-volatile compounds on pre-existing particles.

Factor 5 is dominated by ozone (95%), and moderate explained variation of methane (38%), NMHCs (27%), and OC (11%). The PNC contributions were low (3-8%) and primarily in the smaller sizes (20-50 nm). The diurnal cycle is the mirror image of factor 3, presenting a large peak during the afternoon. Polar plot indicates increased levels for high speed winds (>7 m s^{-1}) blowing from most directions. This factor represents O_3-rich air masses advected in NYC during higher wind speeds. It is likely of regional origin as shown by CWT maps with increased concentrations when air masses pass over the Ohio River Valley and the East U.S. coast. While North America transport may be related to the generation of ozone from the biogenic O_3-precursors emitted from conifer forests, the origin from the coast may be linked to a recirculation zone.

3.2.2 Transition periods

The factors for the transition periods are similar to those for winter. Factor 1 represents secondary particles. However, its contribution to total PNC is much higher (21-25%). It shows higher contributions to the larger particle size bins (>100 nm), $PM_{2.5}$ (81%), sulfate (76%), and OC (78%) with moderate EC (22%), NO_2 (23%), and SO_2 (22%) explained variation. Similar to winter: (i) its diurnal pattern presents a broad minimum during daytime, which is likely related to the mixing layer height dynamics; (ii) polar plot roughly shows increases for low wind speeds (<5 m s^{-1}); (iii) it is strongly correlated with secondary aerosol sources for $PM_{2.5}$ mass (Table 2), but also with biomass burning and road traffic; and (iv) CWT map points to the lower Mississippi River basin as a strong potential source region.

Factor 2 (primary traffic emissions) is also similar to winter: (i) it contributes to 3-8% of total PNC; (ii) it is dominated by NO (100%), but also has significant shares of EC (32%), CO, NMHCs and SO_2 (16-17%); (iii) the daily/weekly cycles show a sharp peak between morning rush hours and a drop on Saturdays; (iv) polar plot clearly indicates increased concentrations during wind calm periods; and (v) it is strongly correlated with road traffic emissions, residual oils and zinc factors. Also in this case, factor 2 may depict the road traffic emissions.

The profiles, polar plot, and daily/weekly patterns of factor 3 are similar to winter. However, it presents lower shares of PNC in the smaller size bins and its contribution to the total PNC is also lower (13-19%). Since outdoor air temperatures are higher in the transition periods

463 compared to winter, the lower concentrations (~1/4 of winter) supports the hypothesis that this
464 factor may also have a contribution from the use of residual oil for space heating in Manhattan.
465 Factor 4 contributes to 48-57% of total PNC and its profile is dominated by particles
466 ranging over a wide size interval (20-200 nm), while the pattern of gaseous pollutants shows
467 significant values for NO_2 (22%) and SO_2 (35%). The polar plot suggests a local origin, showing
468 increased concentrations for low winds. Similar to winter, this factor depicts the local nucleation
469 events, likely driven largely by direct emissions from road traffic during morning rush hours.
470 The O_3-rich aerosol profile matches well with that of winter profile, total PNC
471 explained variation, polar plot, and CWT maps. However, it can be noted that its daily maximum
472 lasts ~2 h more in the late afternoon: this is attributable to the more extended daylight with
473 respect to the winter period.
474
475 *3.2.3 Summer*
476 Secondary aerosol (factor 1) accounts for 9-10% of total PNC and mainly contributes to
477 particles in the coarser ranges (65% of particles >200 nm) as well as to $PM_{2.5}$ (62%), sulfate
478 (78%), OC (38%) and SO_2 (33%). It strongly correlates with ammonium sulfate, but not with
479 ammonium nitrate (Table 2) since PM-bound nitrate concentrations are low in summer due to
480 evaporation (Schaap et al., 2004). It is relatively constant during the day, although a slight
481 decrease can be noted during afternoon. This pattern fits with the diurnal cycles of sulfate and
482 nitrate particles found in summer 2009 at QC using Aerosol Mass Spectrometry data (Sun et al.,
483 2011;2012). They reported that sulfate slightly increased during daytime and nitrate increased
484 overnight. Polar plot analysis shows evident increases for SW winds. However, this atmospheric
485 pattern may be affected by the sea/land breeze effect, which is more pronounced in summer due
486 to the enhanced solar irradiation. The CWT map shows the Ohio and Tennessee River Valleys as
487 the most probable source areas.
488 Traffic emissions (factor 2) also shows profiles, diurnal/weekly patterns, polar plot, and
489 correlations with $PM_{2.5}$ mass sources very similar to the winter and transition periods. This
490 source remains constant throughout the year with its contribution to total PNC (5%) similar to
491 those in other periods.

Factor 3 is again attributed to the background pollution transported from Manhattan. It presents similar patterns of the $PM_{2.5}$ species and gaseous pollutants as observed in the other seasons. However, there are some key differences:

- The polar plot does not show transport from Manhattan (NW). It is dominated by low wind speeds and a lack of clear directionality in summer likely due to the lack of residual oil burning. These results support the hypothesis that central heating system emissions in Manhattan may have a key role in this factor during the cold season. In addition, wind directionality also suggests that this factor is more local in origin during the summer, likely dominated by local road traffic.
- A larger sized PNC mode (50-200 nm) was found compared to the other season factor 3 profiles that had modes in the 20-50 nm range. Condensation/evaporation/dilution processes are the major mechanisms altering particle size distributions after primary particles in the nucleation range are emitted in the atmosphere (Zhang et al., 2004; Harrison et al., 2016). For example, Zhu et al. (2004) measured particle size distributions at various distances downwind from a major highway. They reported size distributions peaking at <10 nm at all distances (from 30 m up to 300 m from the highway) in winter. However, in summer there was a drop in the smallest particle mode (10-20 nm) as distance increased from the highway. Zhang et al. (2004) modeled these results and concluded that condensation/evaporation and dilution were the major mechanisms in altering aerosol size distributions. Fujitani et al. (2012) showed seasonal differences in modes of the finest particles (<30 nm) collected at a roadside site, i.e. a dominant 10-30 nm peak in winter, which was not found in summer. The larger PNC mode found in summer may be related to the ageing processes of particles in the atmosphere after their emission;
- The daily pattern has a minimum during daytime but lacks a nighttime minimum when compared to winter and transition periods. The diurnal pattern of factor 3 presents two evident peaks in winter; such peaks are still evident during transition periods, but the minimum occurring overnight is less prominent. It can be assumed that the drift in the daily cycles may continue during the summer. The different dynamics of the nighttime mixing layer due to the increased temperatures could be the main reason for this change.
- The total PNC concentration attributed to factor 3 differs among the seasons. Winter shows the higher concentration, with transition periods the lower (drop of ~4-fold) and summer

an intermediate concentration (about half than winter). While the higher winter concentrations were attributed to their higher stability during cold conditions and additional emissions of heating systems (also supported by the change in directionality), nucleation may enhance concentration in summer because of the higher solar irradiation and faster formation of low volatility secondary material.

Factor 4 includes most of the particles in the smallest size ranges (20-50 nm), exhibits a sharp mode in the number distribution at 20-30 nm, and makes the largest contribution to the total PNC (38-40%). This factor shows significant weak positive correlations with road traffic emissions and exhibits a diurnal cycle peaking at 1-2 pm, which does not match with factor 4 for winter and transition periods. The polar plot analysis indicates enhanced levels when winds blow from the SW quadrant, which is consistent with road traffic from Brooklyn, the stack emissions from the oil refinery in NJ, and ship emissions from the Port of Elizabeth, NJ. However, nucleation was predicted to be the dominant source of ultrafine particles in Eastern U.S. during summer (Posner and Pandis, 2015) and the sharp peak at 1-2 pm is strongly related to the solar irradiance. Thus, factor 4 is likely to be driven by early afternoon photochemical nucleation processes (Seinfeld and Pandis, 2006; Zhang et al., 2011). For example, strong afternoon nucleation events peaking at around 1 pm were found in spring and summer months in NE U.S. (e.g., Jeong et al., 2004). The O_3-rich factor shows daily cycles and polar plot similar to the other seasons.

5. CONCLUSIONS

This study has compared source apportionment of airborne particulate matter in NYC using chemical constituent and particle number concentrations measured at an urban site in NYC. The PNC data were collected with a TSI model 3031 with lower resolution in the description of the particle number concentrations compared to prior work using scanning mobility particle sizers. The conclusions to be drawn from this work are:

- $PM_{2.5}$ mass concentrations are dominated by secondary species, i.e. ammonium sulfate (35%) and ammonium nitrate (14%). They also contain significant OC concentrations in profiles, i.e. secondary organic aerosol is shared in such sources. While nitrate decreases in warm periods due to its volatilization, sulfate reach maximum levels in the warmer season.

- Traffic emissions (16%), road dust (14%), and aged sea-salt (9%) also contribute to the $PM_{2.5}$ mass, while residual oil, and fresh sea-salt account for less than 5% each.
- $PM_{2.5}$ number concentrations are dominated by nucleation particles, which are mainly generated through (i) early morning nucleation of primary emissions in winter and transition periods and (ii) early afternoon photochemical processes in summer. Advected pollution from Manhattan and Brooklyn are another major source of ultrafine particles.
- In winter, and in part during transition periods, NYC background pollution is dominated by the burning of residual oil for domestic heating.
- Primary road traffic has only a small contribution to the total PNC emitted locally. However, NYC traffic emissions also contribute to the NYC particle background.
- Secondary aerosol accounts for a small portion of total PNC and continental U.S. is the most probable origin.

The concurrent application of source apportionment methods to both mass and particle number concentrations has provided more detailed information about air quality in NYC than would be available from only one metric. In particular, traffic was found to not account for a large amount of $PM_{2.5}$ mass, but it is the main source of particles in NYC. Most of such particles were not locally generated by primary emissions, but are the result of advection from most trafficked zones. The use of residual oils has a small impact on $PM_{2.5}$ mass. However, it may dominate the PNC in cold periods. This finding is useful in order to plan current and future air quality mitigation strategies in NYC.

ACKNOWLEDGEMENTS

The authors gratefully acknowledge: (i) the NOAA Air Resources Laboratory (ARL) for the provision of the HYSPLIT transport and dispersion model and READY website (http://www.ready.noaa.gov) used in this publication; (ii) U.S. EPA for the provision of chemical speciated data through the CSN.

REFERENCES

Adachi, K., Tainosho, Y., 2004. Characterization of heavy metal particles embedded in tire dust. Environment International 30 (8), 1009-1017.

584 Atkinson, R.W., Fuller, G.W., Anderson, H.R., Harrison, R.M. Armstrong, B., 2010. Urban
585 ambient particle metrics and health: a time-series analysis. Epidemiology 21(4), 501-511.
586 Anderson, J. O., Thundiyil, J. G., Stolbach, A., 2012. Clearing the air: a review of the effects of
587 particulate matter air pollution on human health. Journal of Medical Toxicology 8(2),
588 166-175.
589 Barnes, I., Hjorth, J. Mihalopoulos, N., 2006. Dimethyl sulfide and dimethyl sulfoxide and their
590 oxidation in the atmosphere. Chemical Reviews 106(3), 940-975.
591 Barwise, A.J.G., 1990. Role of nickel and vanadium in petroleum classification. Energy & Fuels
592 4(6), 647-652.
593 Bauer, J.J., Yu, X.Y., Cary, R., Laulainen, N. and Berkowitz, C., 2009. Characterization of the
594 sunset semi-continuous carbon aerosol analyzer. Journal of the Air & Waste Management
595 Association 59(7), pp.826-833.
596 Belis, C.A., Larsen, B.R., Amato, F., El Haddad, I., Favez, O., Harrison, R.M., Hopke, P.K.,
597 Nava, S., Paatero, P., Prévôt, A., Quass, U., Vecchi, R., Viana, M., 2014. European guide
598 on air pollution source apportionment with receptor models. JRC Reference Reports
599 EUR26080 EN
600 Becagli, S., Sferlazzo, D.M., Pace, G., Sarra, A.D., Bommarito, C., Calzolai, G., Ghedini, C.,
601 Lucarelli, F., Meloni D., Monteleone, F., Severi, M., Traversi, R., Udisti, R., 2012.
602 Evidence for heavy fuel oil combustion aerosols from chemical analyses at the island of
603 Lampedusa: a possible large role of ships emissions in the Mediterranean. Atmospheric
604 Chemistry and Physics 12 (7), 3479-3492.
605 Benson, D.R., Yu, J.H., Markovich, A., Lee, S.-H., 2011. Ternary homogeneous nucleation of
606 H2SO4, NH3, and H2O under conditions relevant to the lower troposphere. Atmospheric
607 Chemistry and Physics 11, 4755-4766.
608 Bosco, M.L., Varrica, D., Dongarrà, G., 2005. Case study: inorganic pollutants associated with
609 particulate matter from an area near a petrochemical plant. Environmental Research 99,
610 18-30.
611 Brown, S.G., Eberly, S., Paatero, P. and Norris, G.A., 2015. Methods for estimating uncertainty
612 in PMF solutions: Examples with ambient air and water quality data and guidance on
613 reporting PMF results. Science of the Total Environment 518, 626-635.
614 Bukowiecki, N., Lienemann, P., Hill, M., Furger, M., Richard, A., Amato, F., Prévôt, A.S.H.,
615 Baltensperger, U., Buchmann, B., Gehrig, R., 2010. PM10 emission factors for non-
616 exhaust particles generated by road traffic in an urban street canyon and along a freeway
617 in Switzerland. Atmospheric Environment 44(19), 2330-2340.
618 Carslaw, D.C. K. Ropkins, 2012. openair — an R package for air quality data analysis.
619 Environmental Modelling & Software 27–28, 52–61.
620 Carslaw, D.C., Beevers, S.D., Ropkins, K., Bell, M.C., 2006. Detecting and quantifying aircraft
621 and other on-airport contributions to ambient nitrogen oxides in the vicinity of a large
622 international airport. Atmospheric Environment 40, 5424–5434.
623 Chandrasekaran, S.R., Hopke, P.K., Newtown, M. Hurlbut, A., 2013. Residential-scale biomass
624 boiler emissions and efficiency characterization for several fuels. Energy & Fuels, 27(8),
625 4840-4849.
626 Cheung, K.L., Polidori, A., Ntziachristos, L., Tzamkiozis, T., Samaras, Z., Cassee, F.R., Gerlofs,
627 M. and Sioutas, C., 2009. Chemical characteristics and oxidative potential of particulate
628 matter emissions from gasoline, diesel, and biodiesel cars. Environmental Science &
629 Technology 43(16), 6334-6340.

630 Cheung, K.L., Ntziachristos, L., Tzamkiozis, T., Schauer, J.J., Samaras, Z., Moore, K.F. and
631 Sioutas, C., 2010. Emissions of particulate trace elements, metals and organic species
632 from gasoline, diesel, and biodiesel passenger vehicles and their relation to oxidative
633 potential. Aerosol Science and Technology 44(7), 500-513.
634 Colle B.A., Buonaiuto F., Bowman M. J., Wilson R. E., Flood R., Hunter R., Mintz A., Hill D.,
635 2008. New York City's vulnerability to coastal flooding. Bull. Amer. Meteor. Soc. 89,
636 829–841.
637 Costabile, F., Birmili, W., Klose, S., Tuch, T., Wehner, B., Wiedensohler, A., Franck, U., König,
638 K., Sonntag, A., 2009. Spatio-temporal variability and principal components of the
639 particle number size distribution in an urban atmosphere. Atmospheric Chemistry and
640 Physics 9, 3163-3195.
641 Dutkiewicz, V.A., Qureshi, S., Khan, A., Ferraro, V., Schwab, J., Demerjian, K.L., Husain, L.,
642 2003. Sources of fine particulate sulfate in New York. Atmospheric Environment 38:
643 3179–3189.
644 Finlayson-Pitts, B.J., Pitts, J.N., 2000. Chemistry of the Upper and Lower Atmosphere: Theory,
645 Experiments, and Applications. Academic Press, San Diego, p. 969.
646 Fujitani, Y., Kumar, P., Tamura, K., Fushimi, A., Hasegawa, S., Takahashi, K., Tanabe, K.,
647 Kobayashi, S., Hirano, S., 2012. Seasonal differences of the atmospheric particle size
648 distribution in a metropolitan area in Japan. Science of the Total Environment 437, 339-
649 347.
650 Hand, J. L., Schichtel, B. A., Malm, W. C., Pitchford, M. L., 2012a. Particulate sulfate ion
651 concentration and SO 2 emission trends in the United States from the early 1990s through
652 2010. Atmospheric Chemistry and Physics 12(21), 10353-10365.
653 Hand, J.L., Schichtel, B.A., Pitchford, M., Malm, W.C. Frank, N.H., 2012b. Seasonal
654 composition of remote and urban fine particulate matter in the United States. Journal of
655 Geophysical Research 117(D5).
656 Hays, M.D., Fine, P.M., Geron, C.D., Kleeman, M.J. Gullett, B.K., 2005. Open burning of
657 agricultural biomass: physical and chemical properties of particle-phase emissions.
658 Atmospheric environment 39(36), 6747-6764.
659 Harrison, R.M., Jones, A.M., Gietl, J., Yin, J., Green, D.C., 2012. Estimation of the contributions
660 of brake dust, tire wear, and resuspension to nonexhaust traffic particles derived from
661 atmospheric measurements. Environmental Science & Technology 46, 6523-6529.
662 Harrison, R.M., Jones, A.M., Beddows, D.C.S., Dall'Osto, M., Nikolova, I., 2016. Evaporation
663 of traffic-generated nanoparticles during advection from source. Atmospheric
664 Environment 125, 1-7.
665 Holmes, N.S., 2007. A review of particle formation events and growth in the atmosphere in the
666 various environments and discussion of mechanistic implications. Atmospheric
667 Environment 41, 2183-2201.
668 Hopke, P.K., 2015. Applying Multivariate Curve Resolution to Source Apportionment of the
669 Atmospheric Aerosol. In: 40 Years of Chemometrics –From Bruce Kowalski to the
670 Future, Lavine, et al. (Eds.), ACS Symposium Series; American Chemical Society:
671 Washington, DC, pp 129-157.
672 Hopke, P.K., 2016. Review of receptor modeling methods for source apportionment. Journal of
673 the Air & Waste Management Association, 66, 237-259.
674 Hopke, P.K., Zhou, L., Poirot, R., 2005. Reconciling Trajectory Ensemble Receptor Model
675 Results with Emissions. Environ. Sci. Technol. 39, 7980-7983

Huffman, G.P., Huggins, F.E., Shah, N., Huggins, R., Linak, W.P., Miller, C.A., Pugmire, R.J., Meuzelaar, H.L., Seehra, M.S., Manivannan, A., 2000. Characterization of fine particulate matter produced by combustion of residual fuel oil. Journal of the Air & Waste Management Association 50(7), 1106-1114.

Hsu, Y., Holsen, T.M., Hopke, P.K., 2003. Comparison of hybrid receptor models to locate PCB sources in Chicago. Atmospheric Environment 37, 545-562.

IARC (International Agency for Research on Cancer), 2013. IARC: Outdoor air pollution a leading environmental cause of cancer deaths. International Agency for Research on Cancer Monographs on the evaluation of carcinogenic risks to humans, volume 109. Lyon: International Agency for Research on Cancer. Available at: http://monographs.iarc.fr/ENG/Monographs/vol109/mono109.pdf (last accessed on March 2016).

Janhäll, S., Andreae, M.O. Pöschl, U., 2010. Biomass burning aerosol emissions from vegetation fires: particle number and mass emission factors and size distributions. Atmospheric Chemistry and Physics 10(3), 1427-1439.

Jeong, C.H., Hopke, P.K., Chalupa, D., Utell, M., 2004. Characteristics of nucleation and growth events of ultrafine particles measured in Rochester, NY. Environmental Science & Technology 38(7), 1933-1940.

Kasumba, J., Hopke, P.K., Chalupa, D.C., Utell, M.J., 2009. Comparison of sources of submicron particle number concentrations measured at two sites in Rochester, NY. Science of the Total Environment,407(18), 5071-5084.

Kelly, F.J. and Fussell, J.C., 2012. Size, source and chemical composition as determinants of toxicity attributable to ambient particulate matter. Atmospheric Environment 60, 504-526.

Keene, W. C., Khalil, M. A. K., Erickson, D. J., McCulloch, A., Graedel, T. E., Lobert, J. M., Aucott, M. L., Gong, S. L., Harper, D. B., Kleiman, G., Midgley, P., Moore, R. M., Seuzaret, C., Sturges, W. T., Benkovitz, C. M., Koropalov, V., Barrie, L. A., Li, Y. F., 1999. Composite global emissions of reactive chlorine from anthropogenic and natural sources: reactive Chlorine Emissions Inventory. Journal of Geophysical Research 104, 8429–8440.

Kheirbek, I., Haney, J., Douglas, S., Ito, K., Caputo Jr, S. Matte, T., 2014. The public health benefits of reducing fine particulate matter through conversion to cleaner heating fuels in New York City. Environmental Science & Technology 48(23), 13573-13582.

Kleeman, M. J., Riddle, S. G., Robert, M. A., Jakober, C. A., (2008) Lubricating oil and fuel contributions to particulate matter emissions from light-duty gasoline and heavy-duty diesel vehicles. Environ. Sci. Technol. 42, 235−242.

Kim, E., Hopke, P.K., Edgerton, E.S., 2003. Source identification of Atlanta aerosol by positive matrix factorization, Journal of the Air & Waste Management Association 53, 731-739.

Knibbs, L.D., Cole-Hunter, T. Morawska, L., 2011. A review of commuter exposure to ultrafine particles and its health effects. Atmospheric Environment 45(16), 2611-2622.

Kroll, J.H. and Seinfeld, J.H., 2008. Chemistry of secondary organic aerosol: Formation and evolution of low-volatility organics in the atmosphere. Atmospheric Environment 42(16), 3593-3624.

Lane T.N., Pandis S.N., 2007. Predicted Secondary Organic Aerosol Concentrations from the Oxidation of Isoprene in the Eastern United States. Environmental Science and Technology 41 (11), pp 3984–3990

722 Lanzinger, S., Schneider, A., Breitner, S., Stafoggia, M., Erzen, I., Dostal, M., Pastorkova, A.,
723 Bastian, S., Cyrys, J., Zscheppang, A. Kolodnitska, T., 2016. Associations between
724 ultrafine and fine particles and mortality in five central European cities—Results from the
725 UFIREG study. Environment International 88, 44-52.
726 Lee, A. K. Y., Willis, M. D., Healy, R. M., Wang, J. M., Jeong, C.-H., Wenger, J. C., Evans, G.
727 J., Abbatt, J. P. D., 2015. Single particle characterization of biomass burning organic
728 aerosol (BBOA): evidence for non-uniform mixing of high molecular weight organics
729 and potassium, Atmospheric Chemistry and Physics Discussion 15, 32157-32183.
730 Lewis, E.R., Schwartz, S.E., 2004. Sea Salt Aerosol Production. Mechanisms, Methods,
731 Measurements, and Models. Geophysical Monograph 152. American Geophysical Union,
732 Washington, DC. p. 413.
733 Li, Z., Hopke, P.K., Husain, L., Qureshi, S., Dutkiewicz, V.A., Schwab, J.J., Drewnick, F.,
734 Demerjian, K.L., 2004. Sources of fine particle composition in New York city. Atmos.
735 Environ. 38: 6521-6529.
736 Liao, H., Henze, D.K., Seinfeld, J.H., Wu, S. and Mickley, L.J., 2007. Biogenic secondary
737 organic aerosol over the United States: Comparison of climatological simulations with
738 observations, J. Geophys. Res.: Atmos. 112, D06201.
739 Loomis, D., Grosse, Y., Lauby-Secretan, B., Ghissassi, F. E., Bouvard, V., Benbrahim-Tallaa, L.
740 Guha, N., Baan, R., Mattock, H., Straif, K., 2013. The carcinogenicity of outdoor air
741 pollution. The Lancet Oncology, 14(13), 1262-1263.
742 Lough, G.C., Christensen, C.G., Schauer, J.J., Tortorelli, J., Mani, E., Lawson, D.R., Clark, N.N.
743 and Gabele, P.A., 2007. Development of molecular marker source profiles for emissions
744 from on-road gasoline and diesel vehicle fleets. Journal of the Air & Waste Management
745 Association 57(10), 1190-1199.
746 Lupu, A. Maenhaut, W., 2002. Application and comparison of two statistical trajectory
747 techniques for identification of source regions of atmospheric aerosol species.
748 Atmospheric Environment 36(36), 5607-5618.
749 Masiol M., Hopke P.K., Felton H.D., Frank B.P., Rattigan O.V., submitted. Analysis of major air
750 pollutants and submicron particles in New York City and Long Island. Submitted to
751 Atmospheric Environment
752 Medved, A., Dorman, F., Kaufman, S.L., and Pöcher, A., 2000. A New Corona-based Charger
753 for Aerosol Particles. Journal of Aerosol Science 31, 616-617.
754 Moldanová, J., Fridell, E., Popovicheva, O., Demirdjian, B., Tishkova, V., Faccinetto, A., Focsa,
755 C., 2009. Characterisation of particulate matter and gaseous emissions from a large ship
756 diesel engine. Atmospheric Environment 43 (16), 2632-2641.
757 Moreno, T., Alastuey, A., Querol, X., Font, O., Gibbons, W., 2007. The identification of metallic
758 elements in airborne particulate matter derived from fossil fuels at Puertollano, Spain.
759 International Journal of Coal Geology 71, 122-128.
760 Moreno, T., Querol, X., Alastuey, A., de la Rosa, J., Sanchez de la Campa, A.M., Minguillon,
761 M., Pandolfi, M., Gonzalez-Castanedo, Y., Monfort, E., Gibbons, W., 2010. Variations in
762 vanadium, nickel and lanthanoid element concentrations in urban air. Science of the Total
763 Environment 408 (20), 4569-4579
764 NYC Department of Health and Mental Hygiene, 2013a. New York City Trends in Air Pollution
765 and its Health Consequences. New York City Department of Health and Mental Hygiene,
766 New York, NY.

NYC Department of Health and Mental Hygiene, 2013b. Air Pollution and the Health of New Yorkers: The Impact of Fine Particles and Ozone. New York City Department of Health and Mental Hygiene, New York, NY.

NYCCAS, 2016a. Spatial Variation of Fine Particle Vanadium and Ship Emissions in New York City. New York City Community Air Survey (NYCCAS). Available at: https://www1.nyc.gov/assets/doh/downloads/pdf/eode/nyccas-ship-report.pdf [last accessed: July 216]

NYCCAS, 2016b. Nickel Concentrations in Ambient Fine Particles: Winter Monitoring, 2008-2009. New York City Community Air Survey (NYCCAS). Available at: https://www1.nyc.gov/assets/doh/downloads/pdf/eode/nyccas-ni-report0510.pdf [last accessed: July 216]

NYSERDA, 2010. Determination of sulfur and toxic metals content of distillates and residual oil on the State of New York. Final report 10-31, December 2010. New York State Energy Research and Development Authority. Available at: https://www.nyserda.ny.gov/-/media/Files/Publications/Research/Environmental/determination-sulfur-toxic-metals.pdf [last accessed: July 2016]

Ogulei, D., Hopke, P.K. and Wallace, L.A., 2006. Analysis of indoor particle size distributions in an occupied townhouse using positive matrix factorization. Indoor Air 16(3), 204-215.

Ogulei, D. , Hopke, P.K. , Chalupa, D.C., Utell, M.J., 2007. Modeling source contributions to submicron particle number concentrations measured in Rochester, New York. Aerosol Science & Technology 41, 179-201.

Osan, J., Torok, S., Fekete, J., Rindby, A., 2000. Case study of the emissions from a heavy-oil-fueled Hungarian power plant. Energy and Fuels 14, 983–986.

Ostro, B., Hu, J., Goldberg, D., Reynolds, P., Hertz, A., Bernstein, L. Kleeman, M.J., 2015. Associations of Mortality with Long-Term Exposures to Fine and Ultrafine Particles, Species and Sources: Results from the California Teachers Study Cohort. Environmental Health Perspectives 123(6), 549-556.

Paatero, P., 1997. Least squares formulation of robust non-negative factor analysis. Chemom. Intell. Lab. 37, 23-35.

Paatero, P., Tapper, U., 1994. Positive matrix factorization: a non-negative factor model with optimal utilization of error estimates of data values. Environmetrics 5, 111-126.

Paatero, P., Hopke, P.K., 2003. Discarding or Downweighting High-Noise Variables in Factor Analysis Models, Anal. Chim. Acta 490, 277-289.

Paatero, P., Hopke, P.K., Song, X., Ramadan, Z., 2002. Understanding and controlling rotations in factor analytic models. Chemometrics and Intelligent Laboratory Systems 60, 253-264.

Paatero P, Hopke PK, Begum BA, Biswas SW. 2005. A Graphical diagnostic method for assessing the rotation in factor analytical models of atmospheric pollution. Atmospheric Environment 39, 193–201.

Paatero, P., Eberly, S., Brown, S.G., Norris, G.A., 2014. Methods for estimating uncertainty in factor analytic solutions. Atmospheric Measurement Techniques 7, 781-797.

Pant, P., Harrison, R.M., 2013. Estimation of the contribution of road traffic emissions to particulate matter concentrations from field measurements: a review. Atmospheric Environment 77, 78-97.

Peltier, R.E., Hsu, S.I., Lall, R. and Lippmann, M., 2009. Residual oil combustion: a major source of airborne nickel in New York City. Journal of Exposure Science and Environmental Epidemiology 19(6), 603-612.

Pekney, N. J., Davidson, C. I., Zhou, L., Hopke, P. K., 2006. Application of PSCF and CPF to PMF-Modeled Sources of PM2.5 in Pittsburgh. Aerosol Science & Technology 40(10), 952-961.

Pinder, R. W., Dennis, R. L., Bhave, P. V., 2008. Observable indicators of the sensitivity of PM2.5 nitrate to emission reductions—Part I: Derivation of the adjusted gas ratio and applicability at regulatory-relevant time scales, Atmospheric Environment 42, 1275–1286.

Polissar, A.V., Hopke, P.K., Paatero, P., Malm, W.C., Sisler, J.F., 1998. Atmospheric aerosol over Alaska 2. Elemental composition and sources. J. Geophys. Res. 103(D15), 19045-19057.

Posner, L.N., Pandis, S.N., 2015. Sources of ultrafine particles in the Eastern United States. Atmospheric Environment 111, 103–112.

Raaschou-Nielsen, O., Andersen, Z.J., Beelen, R., Samoli, E., Stafoggia, M., Weinmayr, G., Hoffmann, B., Fischer, P., Nieuwenhuijsen, M.J., Brunekreef, B. Xun, W.W., 2013. Air pollution and lung cancer incidence in 17 European cohorts: prospective analyses from the European Study of Cohorts for Air Pollution Effects (ESCAPE). The lancet oncology 14(9), 813-822.

Reff, A., Eberly, S.I., Bhave, P.V., 2007. Receptor modeling of ambient particulate matter data using positive matrix factorization: review of existing methods. Journal of the Air & Waste Management Association 57, 146-154.

Rolph, G.D., 2016. Real-time Environmental Applications and Display sYstem (READY) Website (http://www.ready.noaa.gov). NOAA Air Resources Laboratory, College Park, MD.

Rossi,M.J., 2003. Heterogeneous reactions on salts. Chemical Reviews 103, 4823-4882

Salma, I., Füri, P., Németh, Z., Balásházy, I., Hofmann, W., Farkas, Á., 2015. Lung burden and deposition distribution of inhaled atmospheric urban ultrafine particles as the first step in their health risk assessment. Atmospheric Environment 104, 39-49.

Sánchez de la Campa, A.M., Moreno, T., De La Rosa, J., Alastuey, A., Querol, X., 2011. Size distribution and chemical composition of metalliferous stack emissions in the San Roque petroleum refinery complex, southern Spain. Journal of Hazardous Materials 190(1), 713-722.

Schaap, M., Spindler, G., Schulz, M., Acker, K., Maenhaut,W., Berner, A., et al., 2004. Artefacts in the sampling of nitrate studied in the "INTERCOMP" campaigns of EUROTRAC-AEROSOL. Atmos. Environ. 38, 6487-6496.

Seinfeld, J.H., Pandis, S.N., 2006. Atmospheric Chemistry and Physics: From Air Pollution to Climate Change, second ed. John Wiley & Sons, NewYork.

Shi, L., Zanobetti, A., Kloog, I., Coull, B.A., Koutrakis, P., Melly, S.J. Schwartz, J.D., 2015. Low-concentration PM2. 5 and mortality: Estimating acute and chronic effects in a population-based study. Environmental Health Perspectives 124(1), 46-52.

Sippula, O., Hokkinen, J., Puustinen, H., Yli-Pirila, P., Jokiniemi, J., 2009. Comparison of particle emissions from small heavy fuel oil and wood-fired boilers. Atmospheric Environment 43 (32), 4855-4864.

Solomon, P.A., Crumpler, D., Flanagan, J.B., Jayanty, R.K.M., Rickman, E.E., McDade, C.E., 2014. US National PM2. 5 Chemical Speciation Monitoring Networks—CSN and IMPROVE: Description of networks. Journal of the Air & Waste Management Association,64(12), 1410-1438.

Song, C.H. Carmichael, G.R., 1999. The aging process of naturally emitted aerosol (sea-salt and mineral aerosol) during long range transport. Atmospheric Environment 33(14), 2203-2218.
Squizzato S., Masiol M., 2015. Application of meteorology-based methods to determine local and external contributions to particulate matter pollution: A case study in Venice (Italy). Atmospheric Environment 119, 69-81.
Stein, A.F., Draxler, R.R, Rolph, G.D., Stunder, B.J.B., Cohen, M.D., and Ngan, F., 2015. NOAA's HYSPLIT atmospheric transport and dispersion modeling system. Bulletin of the American Meteorological Society 96, 2059-2077.
Stockwell, W.R., 1994. The effect of gas-phase chemistry on aqueous-phase sulfur dioxide oxidation rates. Journal of Atmospheric Chemistry 19, 317-329.
Stockwell, W.R., Calvert, J.G., 1983. The mechanism of the HO-SO2 reaction. Atmospheric Environment 17, 2231-2235.
Stohl A., 1996. Trajectory statistics—a new method to establish source–receptor relationships of air pollutants and its application to the transport of particulate sulfate in Europe. Atmospheric Environment 30, 579–587.
Stohl, A., 1998. Computation, accuracy and applications of trajectories- review and bibliography. Atmospheric Environment 32, 947-966.
Strak, M.M., Janssen, N.A., Godri, K.J., Gosens, I., Mudway, I.S., Cassee, F.R., Lebret, E., Kelly, F.J., Harrison, R.M., Brunekreef, B. and Steenhof, M., 2012. Respiratory health effects of airborne particulate matter: the role of particle size, composition, and oxidative potential-the RAPTES project. Environmental Health Perspectives, 120(8), pp.1183-1189.
Stelson, A.W., Seinfeld, J. H., 1982. Relative humidity and temperature dependence of the ammonium nitrate dissociation constant, Atmospheric Environment 16, 983–992..
Sun, Y. L., Zhang, Q., Schwab, J. J., Chen, W. N., Bae, M. S., Lin, Y. C., Hung, H. M., Demerjian, K. L., 2011. A case study of aerosol processing and evolution in summer in New York City, Atmospheric Chemistry and Physics 11, 12737–12750.
Sun, Y.L., Zhang, Q., Schwab, J.J., Yang, T., Ng, N.L. Demerjian, K.L., 2012. Factor analysis of combined organic and inorganic aerosol mass spectra from high resolution aerosol mass spectrometer measurements. Atmospheric Chemistry and Physics 12(18), 8537-8551.
US EPA, 2010. AP-42, 5th ed., Chapter 1: External Combustion Sources; U.S. Environmental Protection Agency, 2010; Vol. 1. Available at: http://www3.epa.gov/ttnchie1/ap42/ch01/final/c01s03.pdf [last accessed on February 2016]
US EPA, 2015. Inventory of U.S. Greenhouse Gas Emissions and Sinks: 1990 – 2013. US EPA document 430-R-15-004. US EPA, Washington DC, USA. Available at: http://www3.epa.gov/climatechange/Downloads/ghgemissions/US-GHG-Inventory-2015-Main-Text.pdf [last accessed on January 2016]
ten Brink, H.M., 1998. Reactive uptake of HNO3 and H2SO4 in sea-salt (NaCl) particles. Journal of Aerosol Science 29, 57-64.
Thorpe, A. Harrison, R.M., 2008. Sources and properties of non-exhaust particulate matter from road traffic: a review. Science of the Total Environment 400(1), 270-282.
Turner, M. C., Krewski, D., Pope III, C. A., Chen, Y., Gapstur, S. M., Thun, M. J., 2011. Long-term ambient fine particulate matter air pollution and lung cancer in a large cohort of never-smokers. Amer. J. Respir. Crit. Care Med., 184, 1374-1381.

Wang, Y., J. Huang, T. J. Zananski, P. K. Hopke, and T. M. Holsen. 2010. Impacts of the Canadian forest fires on atmospheric mercury and carbonaceous aerosols in northern New York. Environ. Sci. Technol. 44 (22): 8435–40.

Wang, Y., Hopke, P.K., Chalupa, D.C., Utell, M.J., 2011. Long-term study of urban ultrafine particles and other pollutants. Atmospheric Environment, 45(40), 7672-7680.

WHO, 2000. Air Quality Guidelines for Europe. European Series No 91,World Health Organization. WHO Regional Publications, Geneva.

Wiedinmyer, C., Quayle, B., Geron, C., Belote, A., McKenzie, D., Zhang, X., O'Neill, S. Wynne, K.K., 2006. Estimating emissions from fires in North America for air quality modeling. Atmospheric Environment 40(19), 3419-3432.

Zhang, K.M., Wexler, A.S., Zhu, Y.F., Hinds, W.C., Sioutas, C., 2004. Evolution of particle number distribution near roadways. Part II: the 'Road-to-Ambient'process. Atmospheric Environment 38, 6655-6665.

Zhang, R., Khalizov, A., Wang, L., Hu, M., Xu, W., 2011. Nucleation and growth of nanoparticles in the atmosphere. Chemical Reviews 112, 1957-2011.

Zhang, X., Kondragunta, S. Roy, D.P., 2014. Interannual variation in biomass burning and fire seasonality derived from Geostationary satellite data across the contiguous United States from 1995 to 2011. J Geophys Res: Biogeo 119(6), 1147-1162.

Zhou, L., Kim, E., Hopke, P.K., Stanier, C.O., Pandis, S., 2004. Advanced factor analysis on Pittsburgh particle size-distribution data special issue of aerosol science and technology on findings from the Fine Particulate Matter Supersites Program. Aerosol Science and Technology, 38(S1), 118-132.

Zhu, Y., Hinds, W.C., Shen, S., Sioutas, C., 2004. Seasonal trends of concentration and size distribution of ultrafine particles near major highways in Los Angeles Special Issue of Aerosol Science and Technology on Findings from the Fine Particulate Matter Supersites program. Aerosol Science and Technology 38(S1), 5-13.

Zielinska, B., Sagebiel, J., McDonald, J.D., Whitney, K., Lawson, D.R., 2004. Emission rates and comparative chemical composition from selected in-use diesel and gasoline-fueled vehicles. Journal of the Air & Waste Management Association 54, 1138-1150.

936 **Table 1.** Source apportionment of total PNC (percentage). Results refer to DISP ranges (min-
937 max).

	Secondary aerosol	Road traffic emissions	NYC background	Local nucleation and condensation	O_3-rich aerosol
Winter	3—4	2—6	47—54	35—42	3—8
Transition	21—25	3—8	13—19	48—57	3—8
Summer	9—10	5	34—35	38—40	2—3

938

939 **Table 2.** Pearson' correlations between PMF factor contributions on PM2.5 mass concentration and PMF factor contributions on PNC
940 at QC. Only correlations statistically significant (at $p<0.05$) are shown; correlation coefficients >0.6 are in bold.
941

	Ammonium sulfate	Ammonium nitrate	Fresh sea-salt	Aged sea-salt	Road traffic	Dust	Biomass burning	Residual oils	Zinc
Winter									
Factor 1	**0.86**	**0.67**			0.57		0.58	0.38	
Factor 2	**0.80**	**0.76**	0.36	-0.33	**0.63**	0.47	0.57	**0.64**	
Factor 3		0.32				0.40		**0.68**	0.39
Factor 4	0.47	0.48					0.39	0.45	
Factor 5	**-0.61**	**-0.65**			-0.51	-0.35	-0.44	**-0.66**	-0.33
Transition									
Factor 1	**0.84**	**0.82**		0.49	**0.66**		**0.86**	0.55	
Factor 2	0.39	0.56			**0.89**		0.36	**0.78**	**0.63**
Factor 3				-0.37	0.38				0.43
Factor 4		0.32			0.37	0.37	0.37	**0.75**	0.34
Factor 5					-0.49			-0.37	-0.48
Summer									
Factor 1	**0.94**	0.34							
Factor 2					**0.69**	0.33		0.48	0.46
Factor 3					**0.75**			0.57	0.40
Factor 4		-0.36			0.44			0.36	
Factor 5	0.53			0.32					

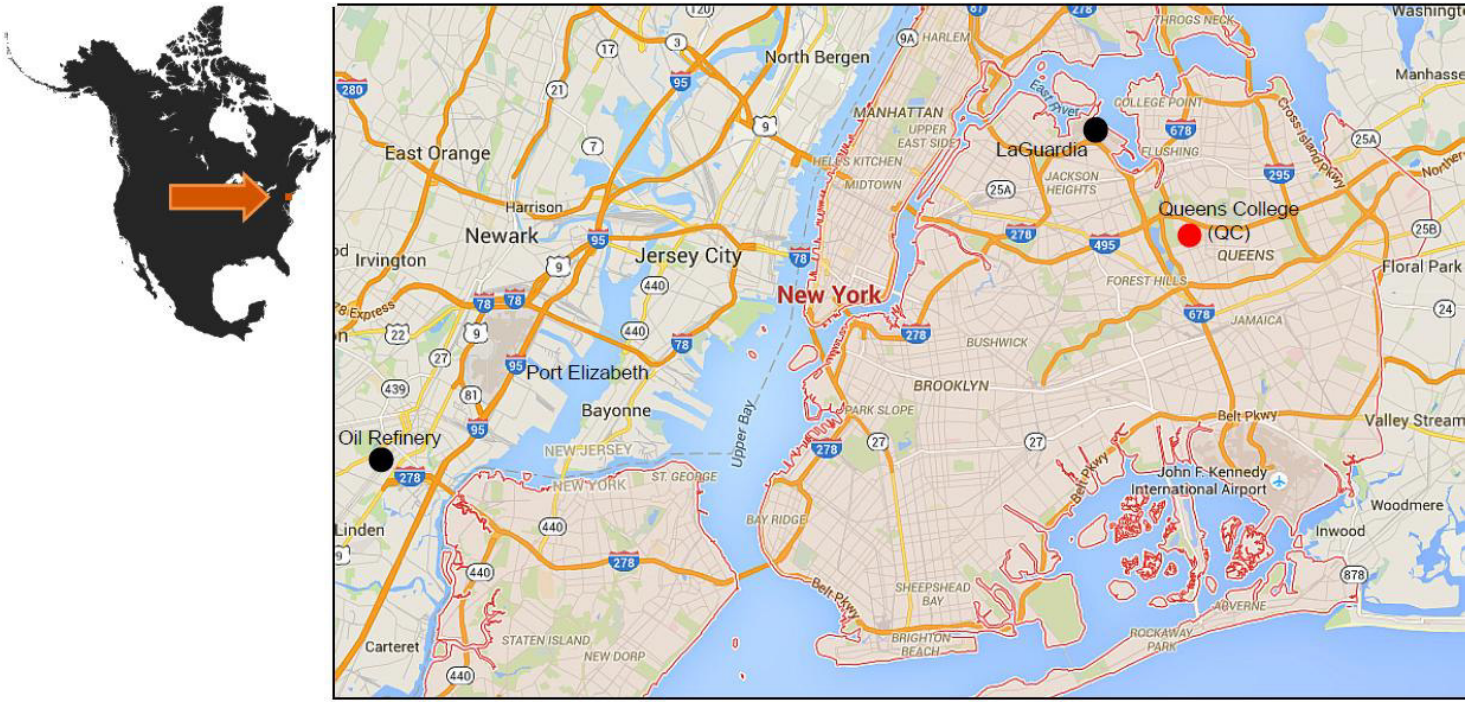

Figure 1. Map of the study area.

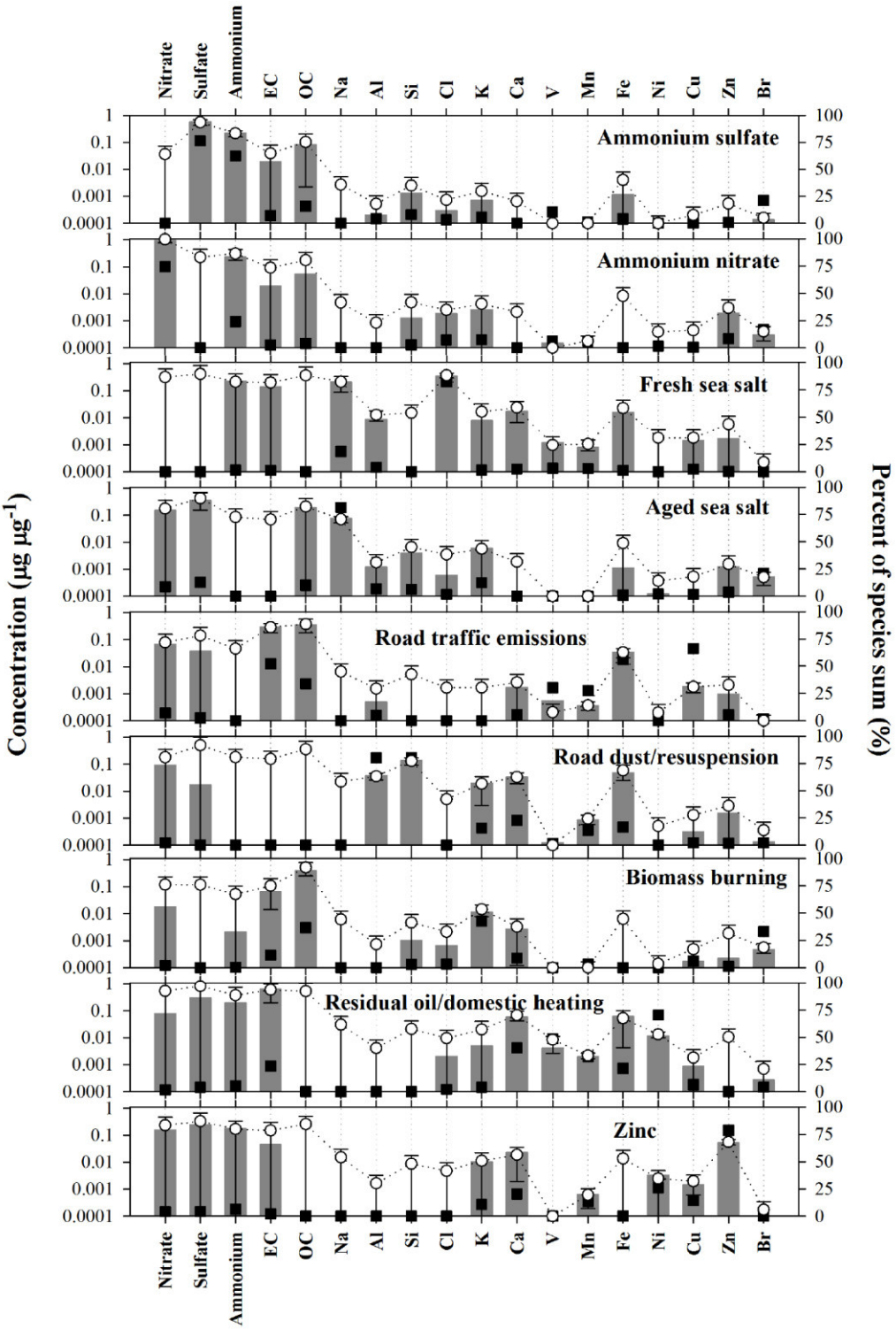

Figure 2. Factor profiles for PMF on chemical-speciated $PM_{2.5}$ mass concentration. Left y-axis: bars represent mass contribution of base run, open circles represent the mean DISP values with the error bars providing the range (minima and maxima values) in of DISP values, the dashed lines are drawn to guide the eye. Right y-axis: filled squares show factor contributions in percent of species sum.

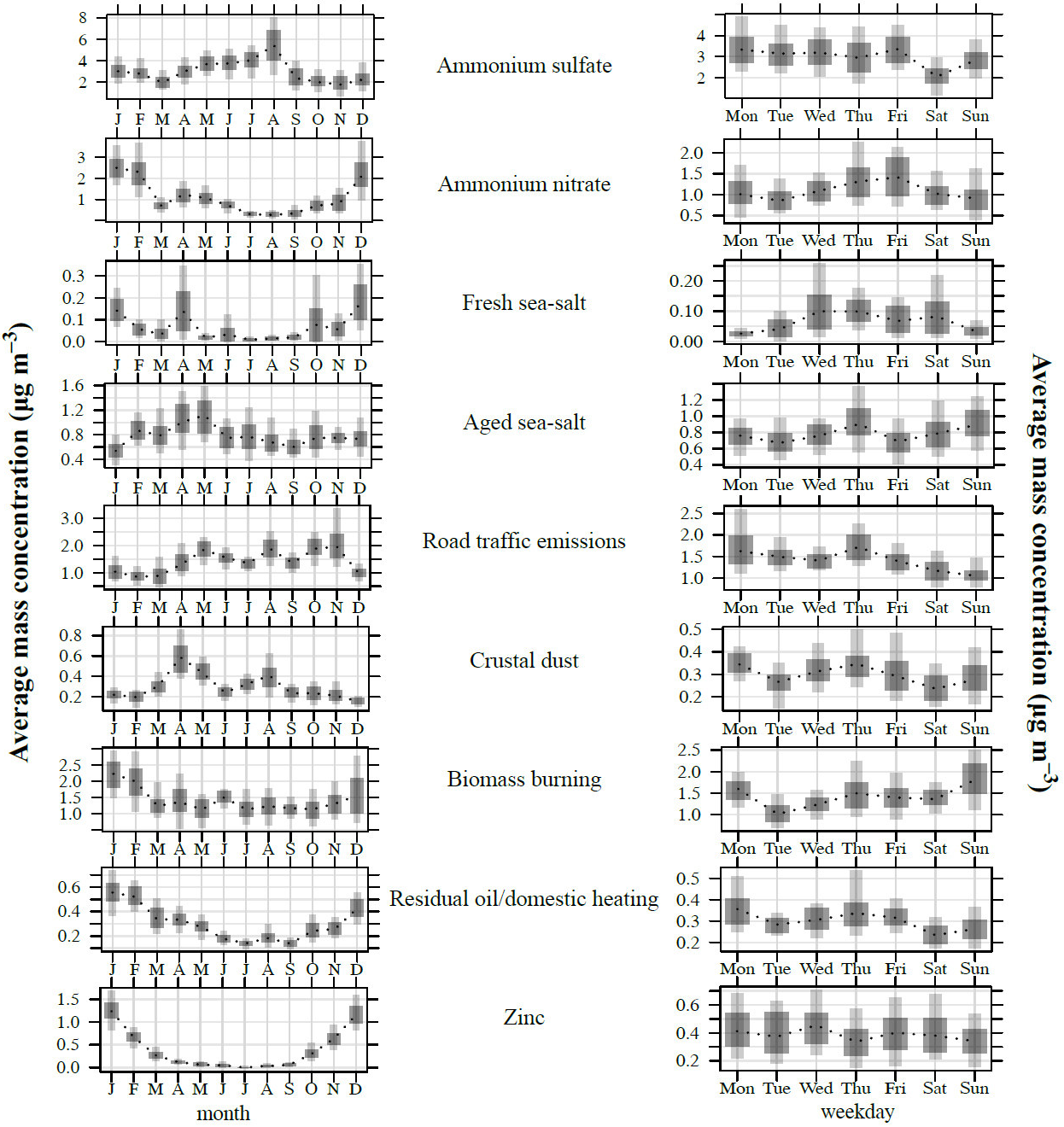

Figure 3. Seasonal and weekly variations of factors extracted from PMF on chemical-speciated $PM_{2.5}$ mass concentration. Each plot reports the average concentrations as a dashed line and the associated 75th and 99th confidence intervals calculated by bootstrapping the data (n=200) as bars.

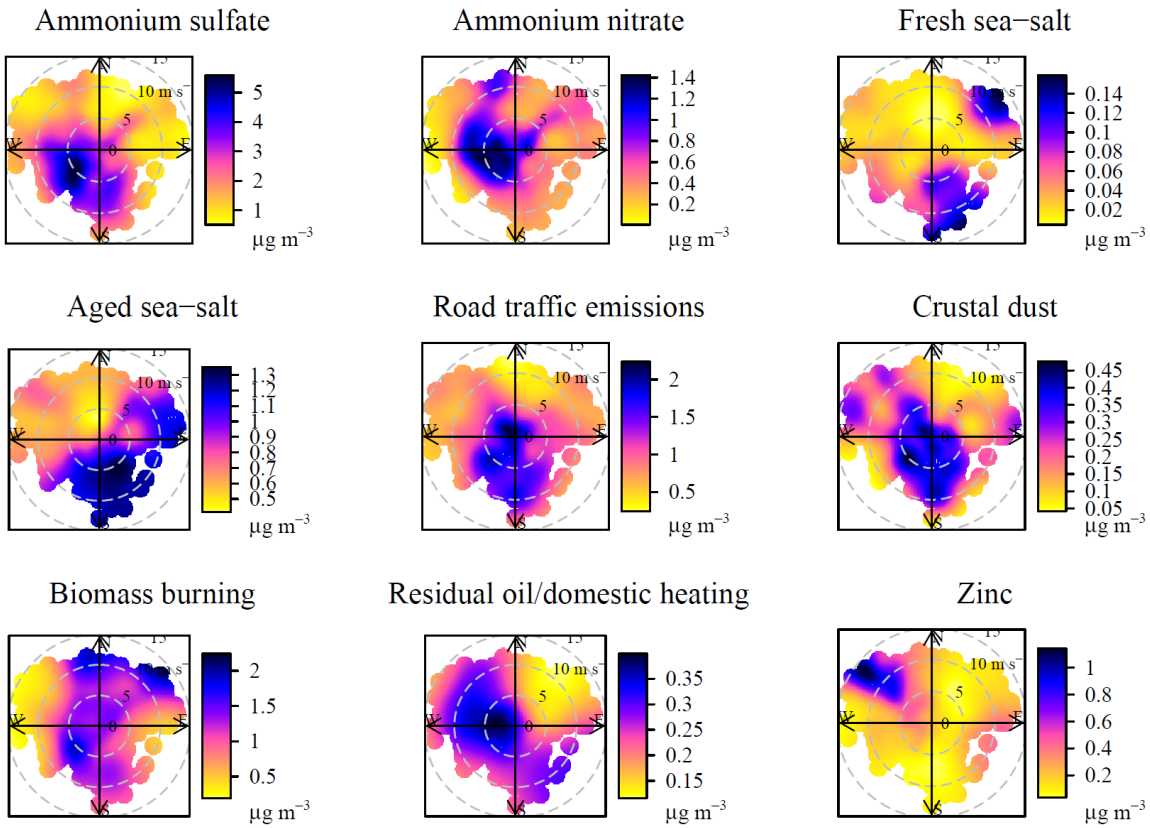

Figure 4. Bivariate polar-plots of PMF sources calculated for chemical-speciated $PM_{2.5}$ mass concentration data. Polar plots scales refer to the average factor contributions to the total variable ($PM_{2.5}$).

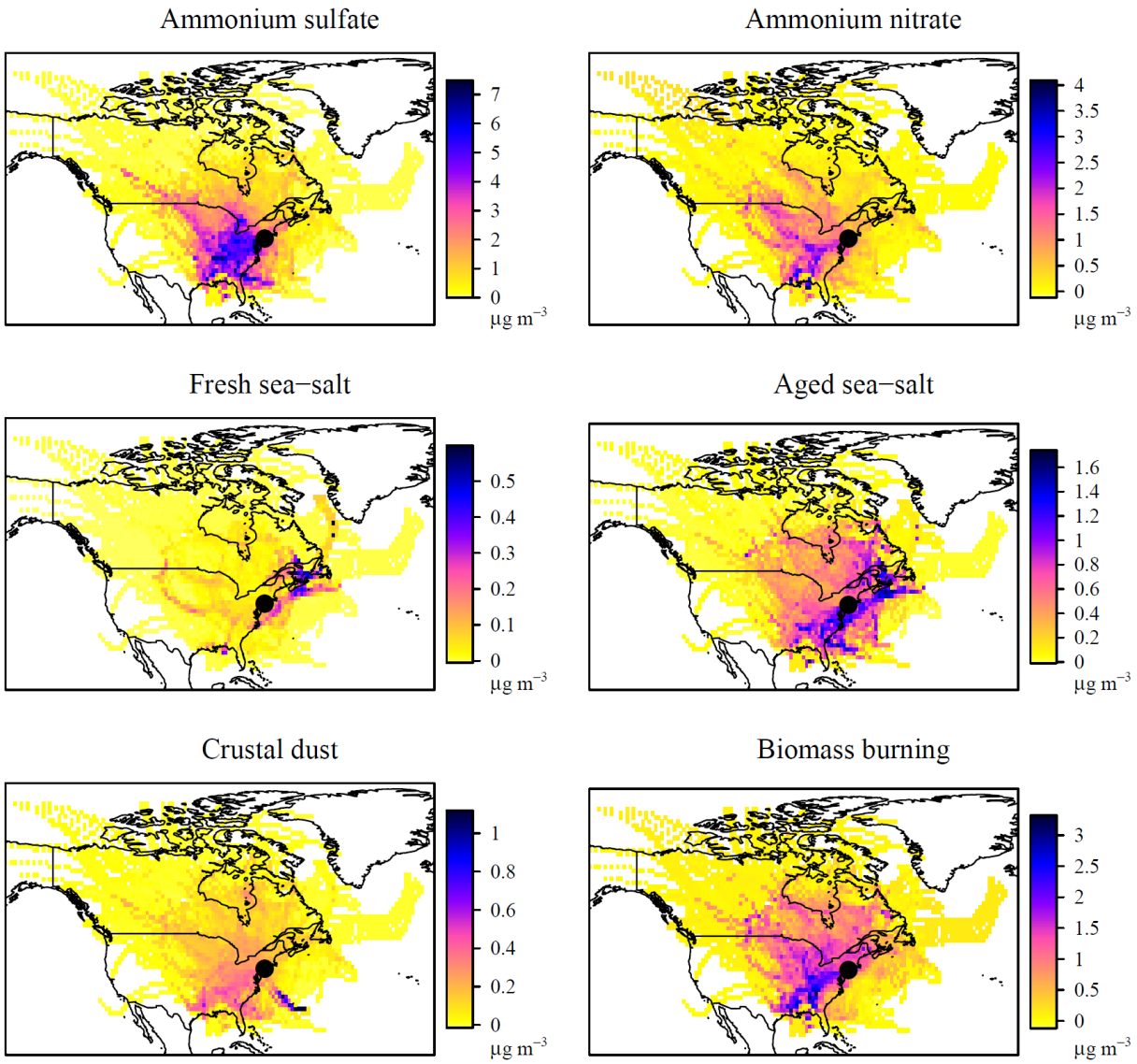

Figure 5. CWT maps of PMF sources calculated for chemical-speciated $PM_{2.5}$ mass concentration data. Map scales refer to the average factor contributions to the total variable ($PM_{2.5}$).

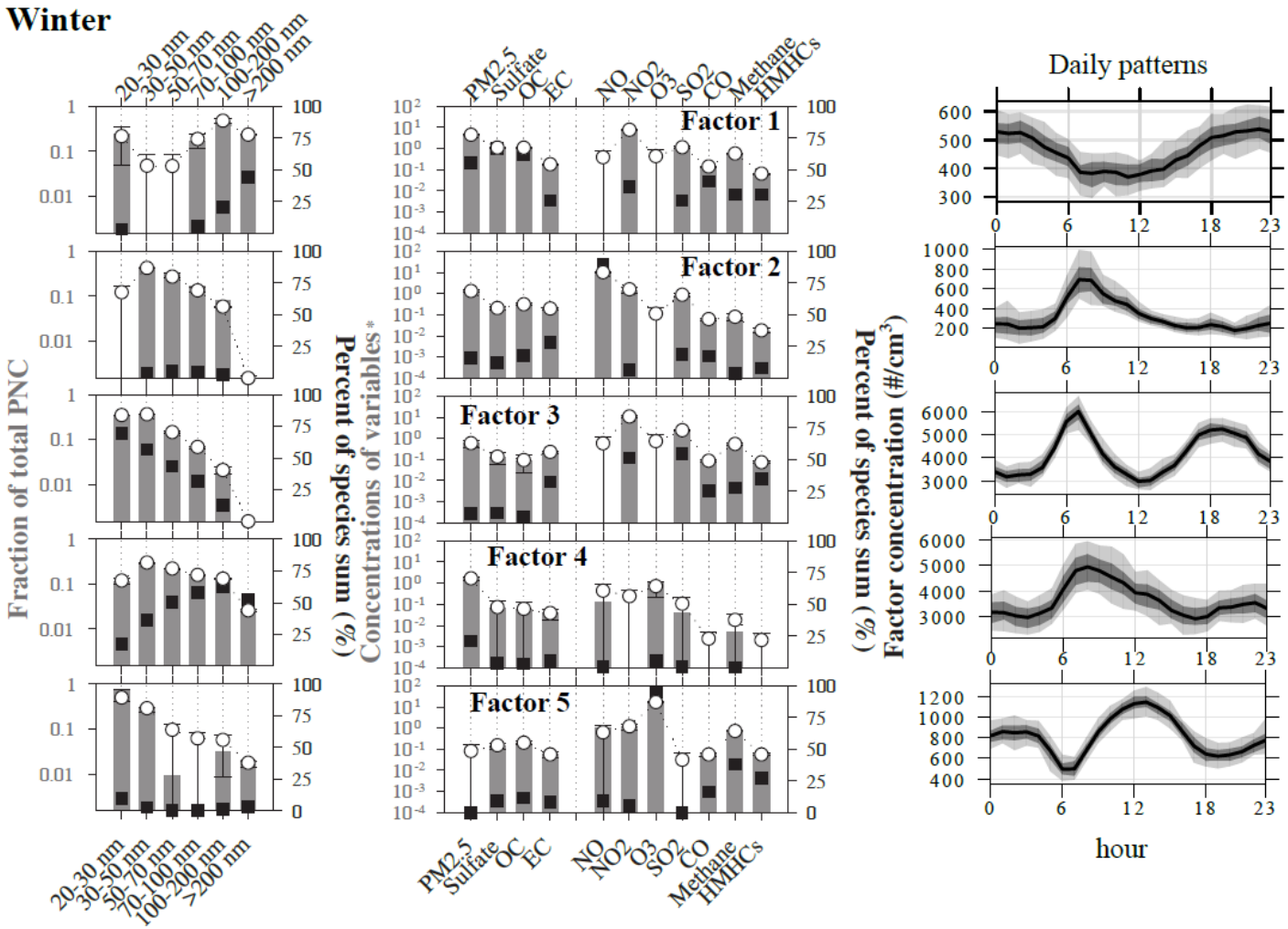

Figure 6. PMF factor profiles for particle number concentration in QC during winter. Filled bars show the profile concentrations; black squares refer to the percentage on the total variable; error bars refer to the range (minima and maxima values) in concentrations calculated by DISP on the base run; white dots are the average of DISP. Note that concentration profiles of PNC are given as fraction of total variable (total PNC), while other variables are in their own units, i.e. ppb for CO, NO, NO_2, SO_2, O_3; ppmC for methane and NMHCs; μg m^{-3} for $PM_{2.5}$, sulfate, OC, EC). Daily profiles are shown (right): average concentrations are provided as solid lines and the associated 75th and 99th confidence intervals calculated by bootstrapping the data (n=200) as shaded areas.

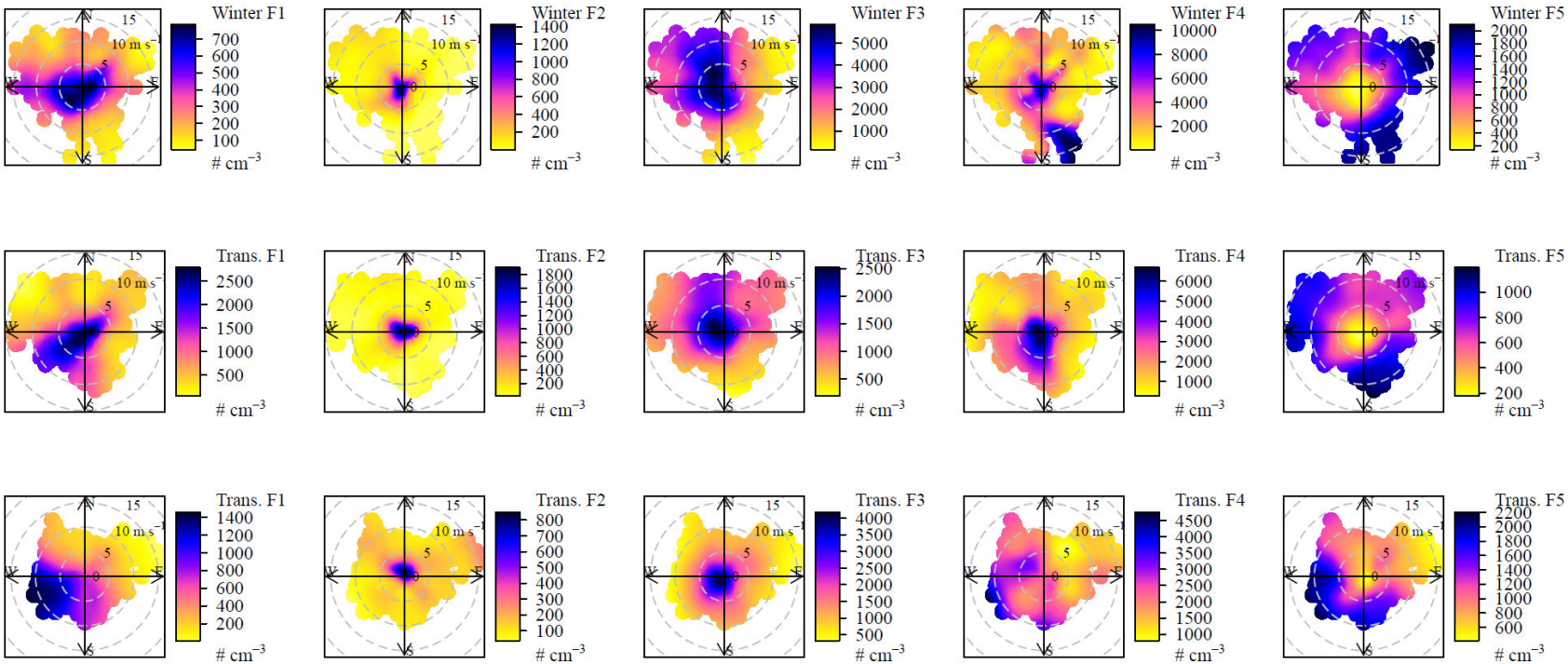

Figure 7. Bivariate polar-plots of all sources extracted by PMF on PNC data. Polar plots scales refer to the average factor contributions to the total variable (total PNC).

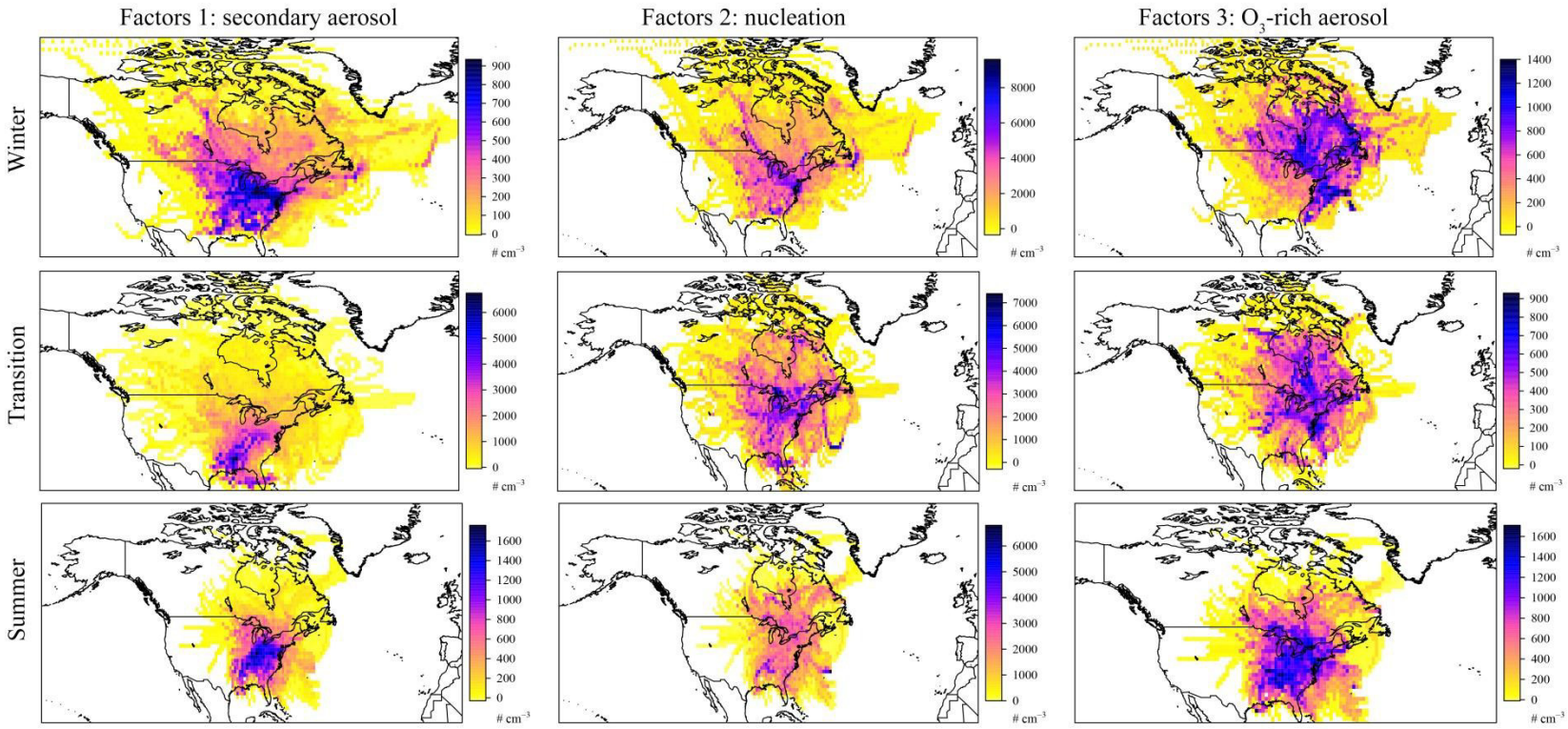

Figure 8. Most important CWT maps of PMF sources calculated on PNC data. Map scales refer to the average factor contributions to the total variable (total PNC).